
# Ethylcellulose-stabilized fat-tissue phantom for quality assurance in clinical hyperthermia

International Journal of Hyperthermia

ISSN: (Print) (Online) Journal homepage: https://www.tandfonline.com/loi/ihyt20

# Ethylcellulose-stabilized fat-tissue phantom for quality assurance in clinical hyperthermia

Mattia De Lazzari, Anna Ström, Laura Farina, Nuno P. Silva, Sergio Curto & Hana Dobšíček Trefná

**To cite this article:** Mattia De Lazzari, Anna Ström, Laura Farina, Nuno P. Silva, Sergio Curto & Hana Dobšíček Trefná (2023) Ethylcellulose-stabilized fat-tissue phantom for quality assurance in clinical hyperthermia, International Journal of Hyperthermia, 40:1, 2207797, DOI: 10.1080/02656736.2023.2207797

**To link to this article:** https://doi.org/10.1080/02656736.2023.2207797



Published online: 17 May 2023.

INTERNATIONAL JOURNAL OF HYPERTHERMIA
2023, VOL. 40, NO. 1, 2207797
https://doi.org/10.1080/02656736.2023.2207797



# Ethylcellulose-stabilized fat-tissue phantom for quality assurance in clinical hyperthermia

Mattia De Lazzari[a], Anna Ström[b], Laura Farina[c], Nuno P. Silva[c], Sergio Curto[d] and Hana Dobšíček Trefná[a]

[a]Biomedical Electromagnetics, Electrical Engineering, Chalmers University of Technology, Göteborg, Sweden; [b]Applied Chemistry, Chemistry and Chemical Engineering, Chalmers University of Technology, Göteborg, Sweden; [c]Translational Medical Device Lab, University of Galway, Galway, Ireland; [d]Department of Radiotherapy, Erasmus MC Cancer Institute, University Medical Center, Rotterdam, The Netherlands

**ABSTRACT**

**Background:** Phantoms accurately mimicking the electromagnetic and thermal properties of human tissues are essential for the development, characterization, and quality assurance (QA) of clinically used equipment for Hyperthermia Treatment (HT). Currently, a viable recipe for a fat equivalent phantom is not available, mainly due to challenges in the fabrication process and fast deterioration.

**Materials and methods:** We propose to employ a glycerol-in-oil emulsion stabilized with ethylcellulose to develop a fat-mimicking material. The dielectric, rheological, and thermal properties of the phantom have been assessed by state-of-the-art measurement techniques. The full-size phantom was then verified in compliance with QA guidelines for superficial HT, both numerically and experimentally, considering the properties variability.

**Results:** Dielectric and thermal properties were proven equivalent to fat tissue, with an acceptable variability, in the 8 MHz to 1 GHz range. The rheology measurements highlighted enhanced mechanical stability over a large temperature range. Both numerical and experimental evaluations proved the suitability of the phantom for QA procedures. The impact of the dielectric property variations on the temperature distribution has been numerically proven to be limited (around 5%), even if higher for capacitive devices (up to 20%).

**Conclusions:** The proposed fat-mimicking phantom is a good candidate for hyperthermia technology assessment processes, adequately representing both dielectric and thermal properties of the human fat tissue while maintaining structural stability even at elevated temperatures. However, further experimental investigations on capacitive heating devices are necessary to better assess the impact of the low electrical conductivity values on the thermal distribution.

**ARTICLE HISTORY**
Received 29 November 2022
Revised 10 April 2023
Accepted 21 April 2023

**KEYWORDS**
Hyperthermia; microwaves; quality assurance; phantom; ethylcellulose

## 1. Introduction

Tissue-mimicking phantoms have a fundamental role in the analysis of interactions between electromagnetic (EM) waves and biological tissues, experimental evaluation of new diagnostic methods, and/or development and testing of medical devices. In the context of hyperthermia therapy (HT), defined as induced temperature increase in the target tissue to 40–44 °C, the availability of appropriate phantom materials is essential to assess the performance of heating devices, their characterization and safety, as well as long term stability in terms of quality assurance (QA) [1].

A phantom is defined as a physical structure made from materials that together mimic the characteristics of a certain biological tissue. In hyperthermia delivered by electromagnetic fields, this encompasses the dielectric properties to reproduce EM wave propagation and thermal properties to represent the distribution of heat in tissues. The majority of the currently available HT devices operate at radio/microwave frequencies between 8 MHz and 915 MHz, dictating the frequency range of interest investigated in this work. Apart from accurate dielectric and thermal properties and the stability of these even at elevated temperatures, other, more practical attributes are important to enable the successful implementation of the phantom in the quality assurance procedures in clinics. These attributes comprise appropriate mechanical properties, stability over time, easily reproducible manufacturing protocols, and finally, accessible, inexpensive, and nontoxic materials [2].

Despite numerous formulations proposed over the past half-century, the ideal phantom is yet to be established. This is especially the case for phantoms representing tissues with low water content, such as fat or bones, that are associated with low permittivity and conductivity. Although not entirely optimal, a handful of phantoms representing high-water content tissues, like muscle and brain, with permittivity ($\varepsilon_r$)

CONTACT Dobšíček Trefná hanatre@chalmers.se Biomedical Electromagnetics, Electrical Engineering, Chalmers University of Technology, Göteborg, Sweden

values ranging between 40 and 80 and conductivity between 0.4–1 S/m in the 10 MHz to 1 GHz range, is available. In these phantoms, the water as a principal component is bound in a network of hydrophilic polymers such as agar [3–6], carrageenan [7,8], polyacrylamide [9], or gelatin [10–12]. Agar-based phantoms are currently recommended in the most recent QA guidelines [13,14] as muscle-mimicking materials, either in a sucrose-agar formulation [15] or in combination with TX-150/1513 gelling powder, also known as Superstuff [5].

Low-water-content tissues that exhibit permittivity between 5 and 26 and low conductivity (0.05–0.4 S/m) for frequencies between 10 MHz and 1 GHz are difficult to mimic by phantoms depending on a high water amount. At the same time, low water amount in gels leads to mechanical weakness. The use of agar-based materials, which require high water content, is limited to approximately $\varepsilon_r = 40$ at frequencies below 1 GHz [15]. Other water-based solutions using alternative net-forming agents have been investigated. Lagendijk and Nilsson [16] proposed a simple-to-make material in the form of dough based on a mixture of water, salt, oil, and flour. The dielectric and mechanical properties at the evaluated frequencies were suitable. Nevertheless, the phantom was subject to rapid degradation over time. Other studies show that oil in water emulsions enforced by gelatin, where oil droplets are kinetically trapped within a gelatin matrix, have the potential to adequately represent the dielectric properties of fat tissue, but their thermal stability has not been described [10–12]. More importantly, the gelation point of these gels is around 25–30 °C, depending on the gelatin percentage by mass used [17]. Recently, Dobšíček Trefná et al. [18] proposed a reinforcement using crystalline nanocellulose in the gelatin gels to increase their thermal stability. Nevertheless, this solution is effective only for QA assessments carried out with radiative heating devices starting at lower temperatures as the phantom weakening occurs already at temperatures above 32 °C. For QA assessment of capacitive devices, the usage of this phantom remains unfeasible due to the high-temperature rise in fatty tissues caused by the preferential power absorption in these tissues at low frequencies [19].

Recipes that avoid the use of water, so-called dry phantoms, have also been explored, but generally, these recipes suffer from complicated preparation procedures, inadequate thermal or dielectric properties, or limited stability over time. Allen et al. [20] proposed a polyester resin (Laminac 4110), acetylene black, and aluminum powder-based material, while another example is a silicone rubber phantom reinforced with carbon fiber [21]. These phantoms are stable over time but demanding to prepare. More recently, Garrett et al. evaluated mixtures of carbon powder and urethane rubber in different quantities, leading to a flexible and dielectrically stable material, but its thermal properties, as well as dielectric properties at frequencies below 1 GHz, have not been investigated [22].

In this work, we propose a new fat-equivalent phantom that is based on an ethylcellulose (EC) gel comprising of glycerol and oil mixture. Despite its ability to form oleogels with high setting and melting temperatures [23–26], the use of EC for the production of solid phantoms has never been reported in the literature. EC is a hydrophobic polymer, meaning that it will be present in the oil phase, and no water is needed in order to disperse the polymer. This is an important difference compared to the gel systems described above [3–8,10–12]. So far, the only use of cellulose derivate in the form of hydroxyethyl cellulose (HEC) has been reported for high permittivity materials [27,28]. Nevertheless, the resulting phantom is viscous. In this work, we demonstrate that EC–glycerol gels have great potential to be routinely employed in QA procedures for HT devices. These fat tissue phantoms meet al.l the requirements in terms of thermal and mechanical properties. The dielectric properties are adequate in the 200–700 MHz band, and if the glycerol concentration is adjusted, even up to 1 GHz. The phantom exhibits a lower conductivity than human fat tissue at low frequencies (8–200 MHz). However, the numerical analysis demonstrates a potential application even for capacitive devices, which needs further experimental verification.

## 2. Materials and methods

The use of the polymer ethylcellulose (EC) as a net-forming agent together with edible oils has been proven to have several applications, for instance, in the food [29] and pharmaceutical [30] fields. In the ethylcellulose oleogel-based fat phantom, we mixed canola oil with glycerol to achieve the appropriate dielectric properties. Canola oil, like most vegetable oils, has both low relative permittivity of about 4 and low conductivity of about 0.02 S/m in the 10 MHz to 1 GHz range [31–34]. Glycerol is a polyol compound that finds applications in the food and cosmetics industry due to its nontoxicity and bacteria resistance. As assessed by Meany et al. [35], pure glycerol has permittivity around $\varepsilon_r = 40$ for frequencies below 1 GHz. Above 1 GHz, its permittivity decreases and stabilizes around $\varepsilon_r = 9$. Its conductivity exhibits moderate values reaching $\sigma = 0.5$ S/m for frequencies below 1 GHz.

### 2.1. Materials and preparation protocol

The phantom is based on an ethylcellulose-glycerol gel, where the main ingredients are oil, glycerol, and ethylcellulose. A regular canola oil, Eldorado, purchased from a local store, was used as the basis for the phantom, in which the ethylcellulose was melted at high temperatures (130 °C). The glycerol was purchased from VWR Chemicals, Radnor, Pennsylvania, USA, while the ethylcellulose Ethocel Standard 45 Premium was provided by Dupont, Grindsted, Denmark. A critical parameter of EC is its viscosity. The values between 41 and 49 mPa·s have been proven effective. The use of ethylcellulose with a higher viscosity may compromise the quality of the mixing procedure, resulting in air engulfment and difficult handling of the phantom due to very rapid solidification.

A dielectric properties assessment revealed that a mixture composed of 57 wt% of glycerol with 7 wt% EC and 36 wt%

of oil creates a mechanically stable gel with an adequate permittivity over the frequency range of interest. As it has been proven through rheological assessments, higher glycerol concentrations have a negative impact on the mechanical stability of the phantom. Therefore, the current permittivity values represent the highest achievable without compromising the mechanical structure of the phantom. However, for frequencies above 700 MHz, the selected concentration of glycerol shows too high conductivity values, as shown in Section 3.1. A later assessment proved that by decreasing the glycerol concentration to 52 wt%, it is possible to adjust the phantom for frequencies above 700 MHz while maintaining acceptable permittivity and satisfactory mechanical properties [36]. The two alternative recipes are reported in Table 1.

The preparation protocol involves the following steps:

1. Oil and glycerol are mixed at room temperature. A head-mixer with adjustable speed is used for this purpose (ME SH-11-6C, MESE, Leeds, England). Alternatively, any other suitable device can be used. Mixing was done so that no air bubbles were visually present in the resulting gel.
2. Once a visually uniform emulsion is obtained, which takes around 10 min, the temperature is gradually increased to 130 °C. A commercially available hot plate is used.
3. The EC is then gradually added to the glycerol–oil mix at 130 °C until EC is visually dissolved.
4. The temperature is now increased to 170 °C to enable the pouring of the compound into the mold without rapid solidification. During this procedure, the pot should be covered to limit the dispersion of hot vapors.
5. The compound is poured into the desired mold and let cool down.
6. Once the mixture cools down, the phantom can be stored either in a refrigerator or in a dry environment, avoiding contact with contaminating agents.

Table 1. concentrations of glycerol, EC, and oil for the two optimized recipes.

| Frequency range of interest | Glycerol [wt%] | EC [wt%] | Oil [wt%] |
|---|---|---|---|
| **<700 MHz** | 57 | 7 | 36 |
| **≥700 MHz** | 52 | 8 | 40 |

Important notice: Keep stirring the mixture continuously during steps 1 to 4 to avoid a glycerol/oil phase separation.

### 2.2. Dielectric properties assessment

The dielectric properties have been assessed using the Dielectric Assessment Kit for Thin Layers (DAK-TL), (Schmid & Partner Engineering AG, Zurich, Switzerland), connected to a Rohde & Schwarz ZNBT8 16 channels vector network analyzer. A schematic representation of the setup is visualized in Figure 1. The sample is placed on a mechanically actuated platform which drives the specimen toward the probe with a force defined by the operator. The measuring device is controlled through dedicated software installed on an external PC, where the measurement data are both displayed and saved. To cover the entire frequency range of interest (8–915 MHz), two different probes have been employed: DAK12-TL2 (frequency range: 4–600 MHz) and DAK3.5-TL2 (frequency range: 200 MHz to 1 GHz), both measuring with a user-defined resolution of 10 MHz. The analyzed phantom samples had a thickness between 8–10 mm and a diameter of at least 80 mm to guarantee the contact between the phantom surface and the entire probe flange. During each measurement, the phantom samples were further pushed toward the probe surface with a constant force of 25 N with the help of the mechanical actuator to guarantee a uniform phantom-probe contact. The dielectric properties have been measured both on the top and on the bottom surface of each sample, in four points on each surface, to assess their uniformity. The average permittivity and conductivity of each sample were then computed.

### 2.3. Thermal properties assessment

The thermal properties have been assessed using a commercial thermal property analyzer (TEMPOS, Meter Group, Inc., Pullman, WA, USA, accuracy: 10%) with the dual-needle sensor (SH-3) [37]. This sensor allows simultaneous measurements of thermal conductivity and volumetric heat capacity in non-liquid materials. The sensor applies a determined quantity of heat to one of the needles for 30 s. The heat is transferred from the needle to the sample under test, and the second needle measures the temperature for 90 s. As described by Silva et al. [38], the thermal property

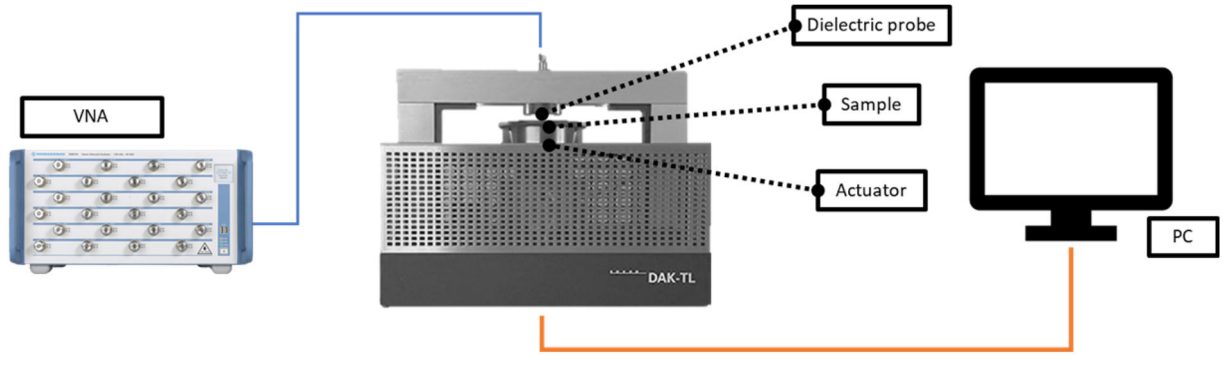


Figure 1. Schematic of the measurement setup for the dielectric properties (DAK-TL2).

parameters are then calculated using an internal algorithm. A cylindrical phantom sample of 7 cm height and 6 cm diameter was used. The entire length of the sensor (3 cm) was inserted into the phantom, ensuring that the minimum dimensions requirements were satisfied [39]. Sets of five measurements were conducted every 15 min to allow the measuring sensor to reach equilibrium before each measurement. Measurements were conducted at room temperature. Before and after each set of five measurements, the sensor was validated through measurements in a Delrin® (Dupont, Grindsted, Denmark) verification block with known thermal properties.

### 2.4. Rheological properties of the EC gels

Rheology is the science of the flow and deformation of matter and describes the interrelation between force, deformation and time. The main purpose of a rheological analysis in this study was to analyze the response of the EC gel upon deformation at different temperatures. As a result, it would provide us with information about the mechanical strength, elasticity and stability at elevated temperatures. The rheological properties of the phantom have been determined using a Discovery HR-3 Rheometer (TA instruments New Castle, US), with a normal force sensitivity of 0.005 N. To determine the maximum possible amount of glycerol in the gel while preserving the mechanical stability of the material, different samples with an increasing weight percentage of glycerol (0%, 50%, 57%, 65%) have been prepared. Prior to the analysis, the phantom samples were liquefied using a hot-air gun and poured into the instrument plate, preheated at 130 °C. The temperature was then reduced to 20 °C, with a rate of 3 °C/min, and afterward increased again to 130 °C, with a rate of 3 °C/min. Storage (G′) and loss modulus (G″) were recorded as a function of temperature and at a fixed frequency of 1 Hz and a strain of 0.5%. The temperature control was assured by a Peltier Plate. For these measurements, a plate-plate geometry was used, with a diameter of 40 mm and a gap of 0.3 mm. The upper plate was equipped with a solvent trap and a custom-made chamber provided by TA Instrument to reduce evaporation and maintain a stable temperature.

### 2.5. Phantom validation in superficial hyperthermia QA procedures

The variation in dielectric and thermal properties of the fat phantom related to the IT'IS tabulated values may impact the values of the performance indicators of the applicator. Therefore, we assessed the impact of varying dielectric properties, as measured in Section 2.2, on performance indicators for superficial applicators. Namely, we considered the following quantities as established in the QA guidelines for superficial hyperthermia [13]:

- **Effective field size (EFS):** the area within 50% of maximum SAR contour in the 1 cm deep plane under the antenna aperture.
- **Thermal effective field size (TEFS):** the area within 50% of maximum temperature rise (TR) contour at 1 cm depth.
- **Thermal effective penetration depth (TEPD):** the depth at which the maximum TR is 50% of the maximum TR at 1 cm depth.

Power and temperature distributions are first calculated using commercially available EM simulation software. The quality indicators are then derived through a MATLAB routine. The effect on EFS, TEFS, and TEPD is assessed numerically for both radiative and capacitive devices, while the results for radiative devices are further validated experimentally.

#### 2.5.1. Numerical assessments

Figure 2 illustrates the arrangements for the validation of both the capacitive and the radiative system as used in the numerical assessment. Simulations were performed with three different sets of dielectric properties of the fat phantom, listed in Table 2. These values correspond to the average, lower, and upper bound of the properties measured on the phantom samples. For comparison, simulation results obtained using the properties defined for the average infiltrated fat tissue in the IT'IS database [40] are included. The thermal properties of the fat phantom followed the measured average values as listed in Table 2, while the parameters of other materials followed the IT'IS database [40].

The thermal parameters are assessed after 6 min of heating, as prescribed by the QA guidelines. Dielectric and

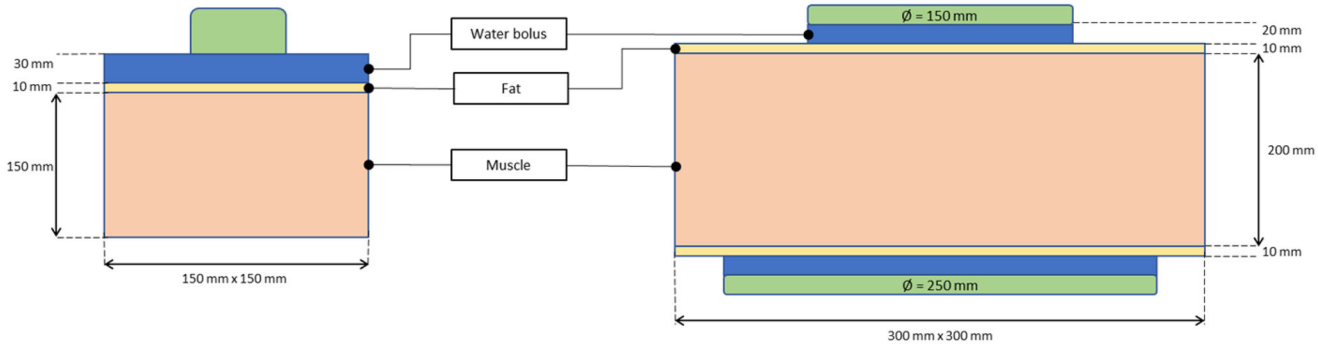


Figure 2. Graphical representation of the geometry adopted for the simulation of an EM radiative system (left) and of a capacitive system (right).

Table 2. Dielectric properties used in the simulation studies for both radiative and capacitive systems.

| | 13.56MHz | | | | | | 434MHz | | | | | |
|---|---|---|---|---|---|---|---|---|---|---|---|---|
| | σ(S/m) | | | $\varepsilon_r$(-) | | | σ(S/m) | | | $\varepsilon_r$(-) | | |
| Air | 0 | | | 1 | | | 0 | | | 1 | | |
| Deionzed Water [40] | 4.23e-5 | | | 84.6 | | | 0.043 | | | 84.6 | | |
| Muscle [40] | 0.63 | | | 138.4 | | | 0.81 | | | 56.9 | | |
| Fat [40] | 0.054 | | | 25.2 | | | 0.082 | | | 11.6 | | |
| Fat (measured) [Lower/Upper range/Average] | 0.001 | 0.002 | 0.0015 | 14.4 | 17.7 | 16.5 | 0.05 | 0.07 | 0.06 | 10.3 | 12.4 | 11.4 |

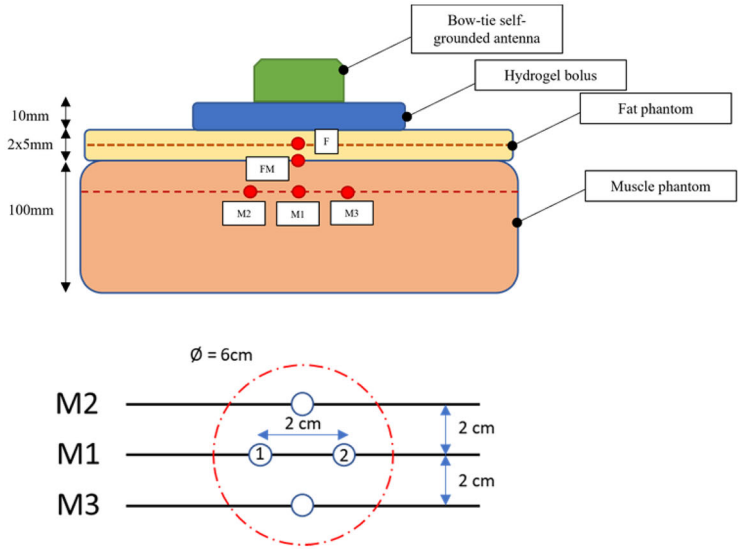


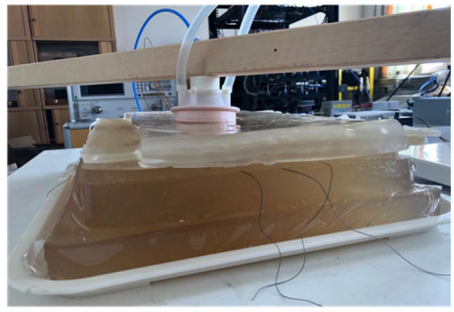

Figure 3. Top left: schematic representation of the experimental setup. The probes position and the geometrical dimensions are indicated. Bottom left: position of the temperature sensors for the probes M1-3, located at 1 cm below the muscle surface, with respect to the antenna aperture (red dotted line). On the right: picture of the same setup.

thermal properties are kept constant during the heating simulation. A percentage variation between the EFS, TEFS, and TEPD values obtained using the different fat models is used as a metric that quantifies the effect of the variation in phantom properties.

*Performance assessment of the EM radiative device.* A self-grounded bow-tie antenna applicator [41] was modeled in CST MW Studio [42] to represent a radiative heating device. The antenna operated at 434 MHz, forwarding a net power of 150 W to a fat-muscle phantom, whose structure is shown in Figure 2. The phantom is composed of a fat-mimicking layer with a uniform thickness of 10 mm, placed on the surface of a 150 mm thick muscle equivalent material. The matching between the antenna and the phantom is guaranteed by a 30 mm thick deionized water bolus. A time-domain solver was used, together with a hexahedral mesh, with an average of 90 000 mesh elements. Open boundary conditions have been applied.

An additional simulation was performed in order to validate the QA experimental results, as described in the next section. The geometry was modified to accurately represent the experimental scenario illustrated in Figure 3. The solver and the meshing setup were identical to the previous scenario. The antenna was set to radiate the power of 87 W at 490 MHz, corresponding with the experimental condition. Permittivity and conductivity of the fat phantom were 10.8[-] and 0.051 S/m, respectively. After a first round of simulations, the power was adjusted to 80 W to compensate for the cable losses and reflections happening in the experimental environment.

*Performance assessment of the EM capacitive device.* A similar configuration was adopted to assess the performance of the EM capacitive HT system, but this time, it was carried out using a simulation platform COMSOL Multiphysics [43], which is more suitable for this simulation and has an easier definition of the feeding port. Following the setup prescribed by the QA guidelines, a 200 mm thick muscle layer is topped on both sides with a 10 mm thick fat phantom layer, see Figure 2. A 20 mm thick deionized water bolus is placed between the electrodes and the phantom. Similarly to Kok et al. [19], two electrodes with diameters of 150 mm and 250 mm are placed at the top and the bottom of the multilayered fat-muscle-fat phantom, respectively. The assumed operation frequency is 13.56 MHz. An initial voltage of 100 V was imposed between the two plates (+50 V and −50 V) and then tuned to reach a temperature rise of at least 6 °C in 6 min at 1 cm depth in the muscle phantom. A frequency-domain study and a time-dependent study have been run to determine the temperature increase in the phantom. The simulation domain was bounded

by an equipotential surface with null voltage. By default for COMSOL, a FEM meshing strategy was adopted, with a total number of elements equal to $5.4 \cdot 10^5$.

#### 2.5.2. Experimental assessment

The phantom was tested for compliance with QA guidelines for superficial HT, following the arrangement described by Dobšíček Trefná et al. [1,13]. A schematic representation and a photograph of the experimental setup are shown in Figure 3.

A 10 mm thick hydrogel bolus (with no temperature control) [44] was employed as a matching medium between the antenna and a $250 \times 380$ mm phantom, consisting of two 5 mm layers of fat equivalent material, placed on a 100 mm thick agar/sucrose muscle phantom [15]. The dielectric properties of the hydrogel bolus at 490 MHz were $\varepsilon_r = 81$ and $\sigma = 0.10$ S/m, while the muscle phantom had $\varepsilon_r = 59$ and $\sigma = 0.69$ S/m.

A self-grounded bow-tie antenna with an aperture diameter of 60 mm was centered on the top of the hydrogel bolus to radiate EM energy for 6 min at the operating frequency of 490 MHz. This frequency was chosen to minimize the antenna reflection, which had a measured value of −11 dB. Initially, a power of 73 W was applied for 60 s, but then increased to 87 W to ensure an adequate temperature rise and kept constant until the end of the experiment. Both phantom and bolus were at room temperature of around 22 °C at the beginning of the experiment.

The temperature rise was monitored at multiple locations by five fiber-optic probes (THR-NS-882X, FISO Technologies Inc, Canada), located in correspondence to the central plane of the antenna, at different depths: between the two fat layers (F, 8 sensors with 1 cm spacing), at the fat-muscle interface (FM, 1 sensor), and 1 cm below the muscle surface (M1–M3, 8 sensors with 2 cm spacing) with a 20 mm spacing between probes. Moreover, the temperature distribution at each interface was captured by an infrared camera (B355, Teledyne FLIR LLC, USA) at the end of the experiment.

## 3. Results

The results reported in this section were obtained by assessing the properties of a phantom containing 57 wt% of glycerol, prepared as described in Section 2.1. The phantom is a semisolid gel, easy to handle, and fairly flexible (Figure 4). Chemically, it is a glycerol-in-oil emulsion, with glycerol droplets kinetically trapped in the oil, while EC acts as a net-forming agent.

### 3.1. Dielectric properties of the EC-glycerol gel

The dielectric properties of the fat phantom over the frequency range of 8 MHz to 1 GHz are presented in Figure 5. The measured average values of permittivity and conductivity on four distinct samples are shown along with the tabulated values of human fat tissues provided by the IT'IS database [40]. Although the infiltrated fat tissue properties are considered in HT treatment planning more often, we added the values for non-infiltrated fat tissue to provide a better impression of the variability in the human body. The plots further indicate the measurement uncertainties, which typically range up to 15% at frequencies below 100 MHz and 5% above 100 MHz [40,45].

Figure 4. A phantom sample used for the QA experimental verification. The material can be easily handled without damaging its structure.

The solid green and blue lines represent the measurements performed using the DAK12-TL2 probe and the DAK35-TL2 probe, respectively, together with their uncertainties. The phantom exhibits an average permittivity that decreases from 17 at low frequencies to 10 at 1 GHz. The conductivity is almost zero at low frequency, reaching values around 0.16 S/m at the other extreme of the range.

It is worth remembering that the data presented in Figure 5 have been obtained from phantom samples with a glycerol concentration of 57 wt%. Lowering the glycerol concentration to 52 wt% allows for adjustment of the conductivity values for frequencies above 700 MHz, in particular targeting for 915 MHz, the other commonly used frequency in hyperthermia systems [36]. For comparison purposes, the average dielectric properties for the two formulations, at 434 MHz and 915 MHz, are reported in Table 3.

The phantom was stored in a wrapped plastic foil in a refrigerator, and its dielectric properties were re-measured after one month without any observable changes.

### 3.2. Thermal properties: thermal conductivity and capacity

The thermal properties of the phantom at room temperature are presented in Table 4. The average value of thermal conductivity (k) and volumetric heat capacity (Cv) of the phantom approximate the ones reported from the IT'IS database [40] as a reference for fat tissue. The average measured thermal conductivity and volumetric heat capacity differ by +13% and +8% from the average expected value. It is worth reminding here that the accuracy of the thermal property analyzer used is 10%. The thermal properties were monitored after one month, and no variations were observed.

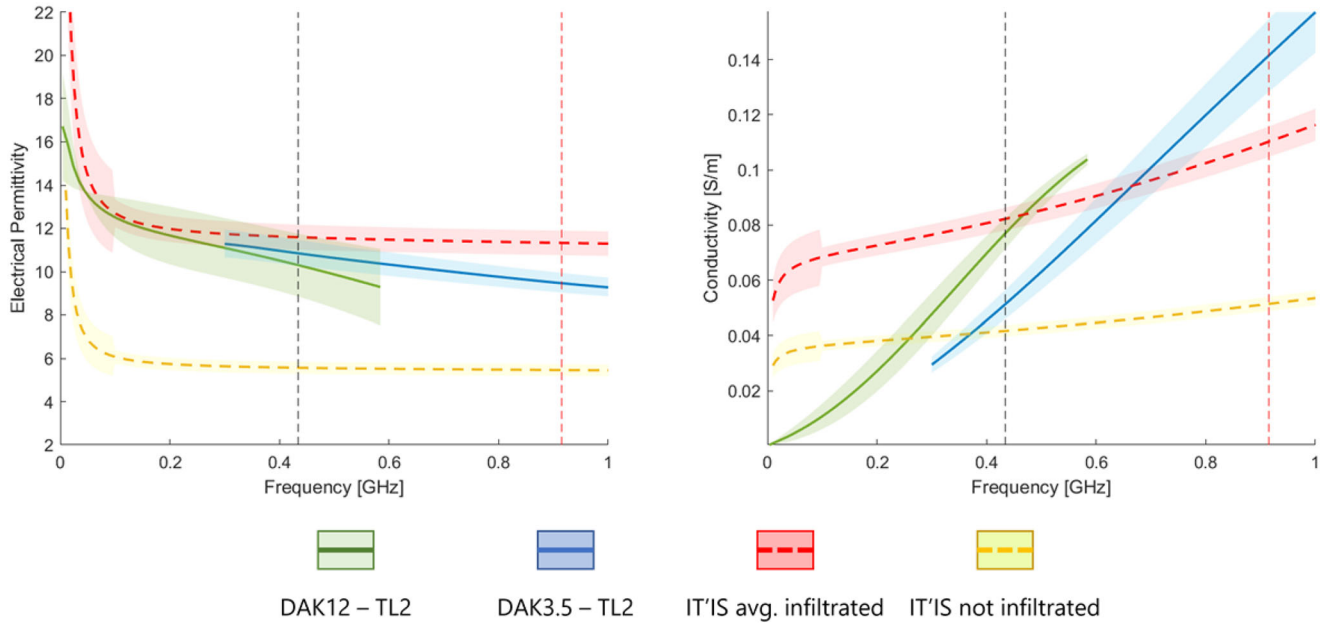


Figure 5. Average permittivity (left) and electrical conductivity (right) of the phantom, using a DAK12-TL2 (green solid line) and a DAK3.5-TL2 (blue solid line), with their confidence intervals. The dashed lines represent the dielectric properties of the average infiltrated fat tissue (red), and non-infiltrated fat tissue (yellow), both taken from the IT'IS database. The corresponding shaded areas indicate the uncertainty of dielectric probe measurements. Two vertical markers are positioned at 434 MHz and at 915 MHz.

Table 3. Average permittivity and conductivity measured values for two different phantom formulations (glycerol concentration: 57 wt% and 52 wt%). The data are reported for two common operating frequencies in HT, 434 MHz and 915 MHz.

| | Permittivity [−] | | Conductivity [S/m] | |
|---|---|---|---|---|
| Frequency | 57 wt% | 52 wt% | 57 wt% | 52 wt% |
| 434 MHz | 11.75 | 7.20 | 0.07 | 0.05 |
| 915 MHz | 9.46 | 5.96 | 0.14 | 0.09 |

Table 4. Measured thermal properties of the phantom at room temperature.

| Property | Reference value for fat tissue [40] | Measured value at 22-24 °C |
|---|---|---|
| **k [W/m/°C]** | 0.21 ± 0.02 | 0.246 ± 0.000 |
| **Cv [J/kg/°C]** | 2.348 ± 0.372 | 2.556 ± 0.002 |

### 3.3. Rheological properties of the EC-glycerol gels

The storage (G′) and loss (G″) moduli of the EC and EC–glycerol gels are shown in Figure 6. The gels were added hot (130 °C) to the rheometer, after which the temperature was lowered to 20 °C. G′ and G″ have similar values at temperatures > 100 °C, showing a paste-like behavior. Once the temperature is lowered < 100 °C, G′ increases faster than G″, showing a more elastic behavior and onset of gelation. G′ and G″ as a function of temperature is similar upon heating and cooling, and the gel melts at similar temperatures as it sets. The general behavior of the gel as a function of temperature is independent of the presence of glycerol or not, however, the absolute values of G′ and G″ differ, as well as gelation onset and melting (Table 5). The addition of glycerol reduces G′ and increases the temperature for the gelation onset. Table 5 lists the moduli values and tan δ (tan δ = G″/G′) at 20 °C and 39 °C for both temperature ramps (cooling and heating) of the EC and EC-glycerol gels. The influence of glycerol upon temperature for setting of the gel as defined here is reported in Table 6.

The values presented in the table clearly show that increasing glycerol content and reducing oil leads to a reduction in G′ independent of temperature and increase in tan δ. The increase in tan δ shows that the elastic component of the gel is reduced while the viscous component increases. The network is thus weakened, and the EC gel becomes more paste-like the more glycerol is added. Table 6 further shows that the setting temperature of the network increases with increased glycerol content of 50 wt%, in agreement with a polymer being driven out of solution, owing to poor solvent quality.

These results suggest how the usage of a glycerol content higher than 57 wt% leads to poorer gel properties (higher tan δ and low G′).

### 3.4. Phantom validation in superficial hyperthermia QA procedures: numerical assessment

The resulting EFS, TEFS, and TEPD obtained from the simulations by considering different fat phantom properties are listed in Table 7. For comparison, we further include the percentage variation with respect to the values calculated for the model, using the IT'IS database values. The results are presented for the three different fat phantom models, representing the lower (LB) and upper bound (UB) of the confidence interval and the average (AVG) values of the measured dielectric properties (Figure 5). The results obtained for the different phantom models generally show a good agreement, in particular for the radiative systems. The maximum difference in the LB case results in an overestimation of EFS and TEFS, about 5.26% and 4.10%, respectively. The TEPD is underestimated by 4.5% in the same case.

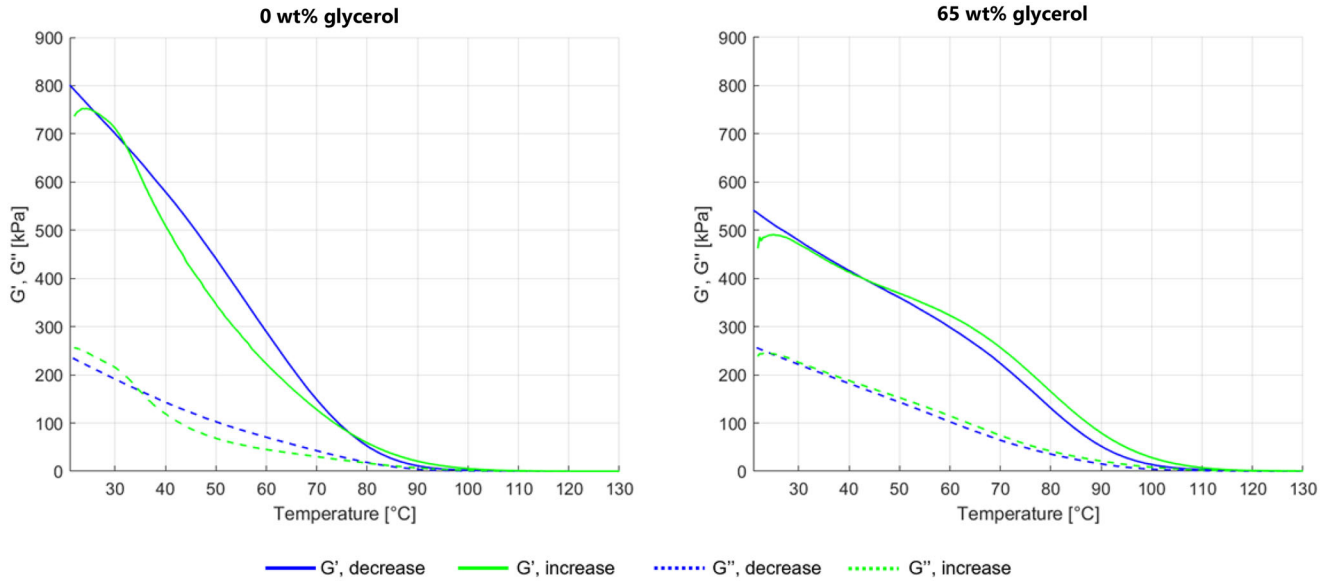


Figure 6. G′ (solid line) and G″ (dashed line) as a function of temperature for different glycerol content phantoms: 0 wt% (left) and 65 wt% (right). The samples were first cooled from 130 °C to 20 °C (blue) and then heated to reach again 130 °C (green).

Table 5. G′ and tan δ at T = 20 and 39 °C for EC and EC glycerol gels. The moduli values were recorded at f = 1 Hz and strain = 0.5%. The different values given are the value obtained upon cooling (C) and heating (H).

| | G′ at 20 °C [kPa] | | tan δ [–] at 20 °C | |
|---|---|---|---|---|
| Glycerol content (wt%) | C | H | C | H |
| 0 | 810 | 750 | 0.3 | 0.4 |
| 50 | 820 | 730 | 0.5 | 0.4 |
| 57 | 680 | 640 | 0.4 | 0.5 |
| 65 | 550 | 490 | 0.5 | 0.6 |
| | G′ at 39 °C [kPa] | | tan δ [–] at 39 °C | |
| Glycerol content (wt%) | C | H | C | H |
| 0 | 810 | 530 | 0.3 | 0.2 |
| 50 | 640 | 630 | 0.5 | 0.4 |
| 57 | 530 | 550 | 0.4 | 0.4 |
| 65 | 420 | 420 | 0.5 | 0.5 |

Table 6. Gel-setting temperature calculated for the different phantom samples with increasing glycerol content.

| Glycerol content (wt%) | Setting point [°C] |
|---|---|
| 0 | 75 |
| 50 | 90 |
| 57 | 90 |
| 65 | 90 |

For capacitive systems, the differences in EFS reach similar values, between 5–6%. The deviations in thermal quality indicators are larger due to preferential heating of the fat at the fat-muscle boundary, typical for capacitive systems. In the most extreme case of LB dataset, the TEFS is overestimated by 13.7% while TEPD is overestimated by 23.5%.

The simulated temperature distribution for radiative and capacitive systems is exemplified in Figure 7, both on the vertical XZ plane and on the horizontal XY place, at 1 cm depth in the muscle. For capacitive systems, the vertical view reveals the final temperature within the fat layer being around four times higher than in the muscle phantom, thus highlighting the importance of the mechanical stability of the phantom material over a large temperature range.

### 3.5. Phantom validation in superficial hyperthermia QA procedures: experimental validation

The temperature increase recorded by thermal sensors during the 6-min exposure at 73 W (0–60 s) and 87 W (60–360 s) is shown in Figure 8. The vertical positions of the temperature probes (F, FM, M1-3), and their horizontal placement in the 1-cm depth of muscle phantom (M1, M2 and M3) are better visualized in Figure 3. The antenna was centered in between sensors 3 and 4 of probe M1 (sensors M1-1 and M1-2, respectively). The results show a temperature increase of around 10 °C for these sensors after 6 min, validating the applicator's thermal capability according to the QA guidelines, which require a minimum increase of 6 °C after 6 min [1]. The small difference between the temperature recorded by these two sensors can be explained by the slight misplacement of the sensors with respect to the antenna center.

The recorded data by probe F reveal a temperature increase of 15 °C between the two fat layers at the end of the heating period, and an increase of about 13 °C at the interface between muscle and fat (FM). In both cases, the sensor was placed right below the antenna center.

Figure 9 shows the thermal images captured by the IR camera after 6 min of exposure and the corresponding simulated temperature distributions between different interfaces. To better visualize the correspondence between the numerical and experimental data, the temperature increase along the X and Y central axes is compared in Figure 10, showing an excellent agreement. The measured temperatures are slightly lower than the simulated ones very likely due to heat dissipation in the phantom that had happened within the 70 s before the IR image was captured. The absolute error of the camera, ±2 °C as stated by the manufacturer, may be another source of uncertainty.

Table 7. EFS, TEFS and TEPD values calculated from the simulated SAR and temperature distribution for a capacitive and a radiative system, adopting different dielectric properties for the fat layer (values from the database, plus lower, higher, and average values measured in the phantom). The percentage difference with respect to the values computed using the IT'IS based fat phantom model is also shown.

| | EFS [cm$^2$] | | | | TEFS [cm$^2$] | | | | TEPD [mm] | | | |
|---|---|---|---|---|---|---|---|---|---|---|---|---|
| Study | IT'IS | LB | UB | AVG | IT'IS | LB | UB | AVG | IT'IS | LB | UB | AVG |
| Radiative | 6.65 | 7.00 | 6.74 | 6.97 | 7.30 | 7.60 | 7.29 | 7.48 | 35.2 | 33.6 | 34.5 | 34.6 |
| Δ% | – | +5.26 | +1.35 | +4.8 | – | +4.10 | +0.14 | +2.4 | – | −4.5 | −2.0 | −2.0 |
| Capacitive | 20.4 | 21.6 | 21.5 | 21.5 | 17.6 | 20.02 | 18.9 | 19.2 | 17.0 | 21.0 | 17.4 | 18.0 |
| Δ% | – | +5.88 | +5.40 | +5.4 | – | +13.7 | +7.3 | +9.0 | – | +23.5 | +2.4 | +5.8 |

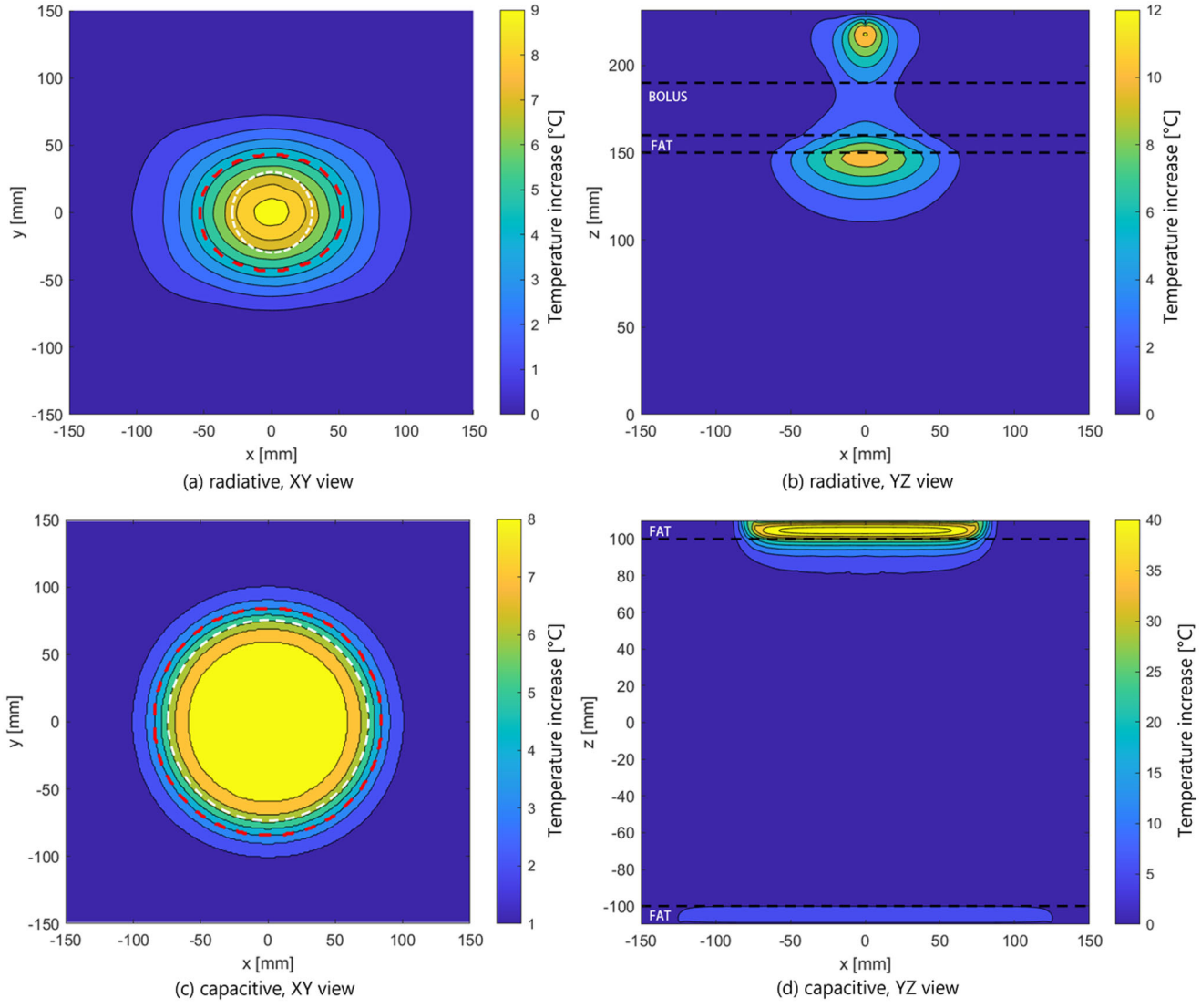


Figure 7. Contour plots of the temperature increase within a fat-muscle phantom after 6 min of heating with a single antenna radiative system (top row) and a two electrodes capacitive system (bottom row), as described in section 2.5.1. Left column: XY plan view at 1 cm depth in the muscle phantom, where the red dotted lines indicate the boundaries of the TEFS and the contours of the antenna and the top electrode are represented as white dotted lines. Right column: XZ view. Here, the boundaries between fat/muscle/bolus are shown as black dotted lines.

## 4. Discussion

This work proposes the use of a glycerol and oil mixture stabilized with ethylcellulose as a fat-tissue mimicking phantom. The objective of this work was to define a generic phantom recipe, suitable for hyperthermia QA assessments over a frequency range of 8–1 GHz.

Overall, the developed phantom is a good candidate to adequately represent human fat tissue, with satisfactory thermal and mechanical properties. The representability of the dielectric properties is limited to the 200–700 MHz range, targeting 434 MHz, but easily extendable to a higher frequency by lowering the glycerol concentration. A stronger limitation appears in the lower frequency range (8–200 MHz). Both permittivity and conductivity values are within the range of interest dictated by reference values for infiltrated and non-infiltrated fat, with the exception of electrical

conductivity at low frequencies. The conductivity of the fat phantom is 0.001 at 8 MHz in comparison to literature values of 0.050, but linearly increases with frequency to become equivalent at frequencies above 200 MHz. In the current protocol, the conductivity values are adjusted by the increased amount of glycerol which is limited by the rheology of the gel. This is obvious from the rheological analysis, revealing an increase in loss tangent (tan $\delta$) when the amount of glycerol is higher than 57 wt%. Another common and simple mechanism to increase the conductivity of the gel could be the addition of NaCl to the solution. Unfortunately, in the case of the NaCl-glycerol mixture, this mechanism becomes effective first at frequencies above 100 MHz [35].

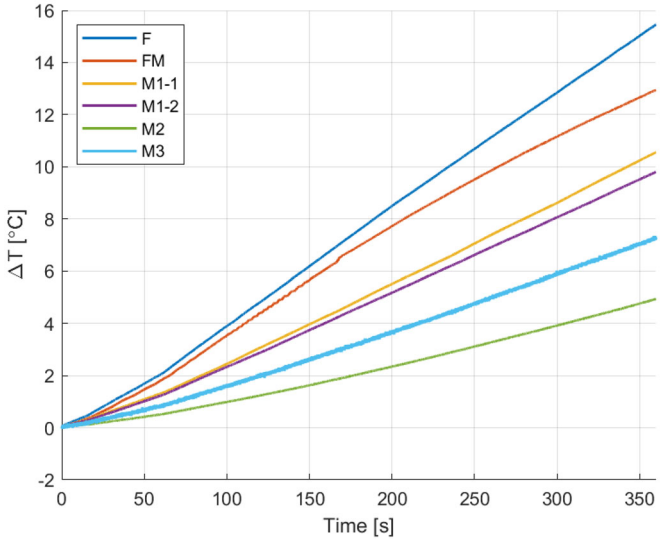


Figure 8. Temperature increase recorded over 6 min by fiber-optic temperature probes at different measurement points. On the right side, the location of the sensors (top) and the location of the probes within the layered phantom (bottom).

The measurement of the dielectric properties of materials characterized by low permittivity and conductivity values with open-ended coaxial dielectric probes is a challenging task, especially at frequencies below 100 MHz, and until recently, not been possible with commercial devices. To assess the dielectric properties within the frequency range of interest, two probes from the Dielectric Assessment Kit for Thin Layers (DAK-TL) have been used, operating at two different but partially overlapping frequency ranges: 4–600 MHz and 200 MHz–20 GHz. Unexpectedly, the properties of the samples measured under the same conditions at frequencies common for both probes were repeatedly different, as visible in Figure 5. Despite independent calibration procedures required for each probe, as indicated by the manufacturer, the differences are surprisingly high. Further verification tests carried out on materials with known properties, such as glycerol, revealed a systematic difference of around 5 to 15% between the values measured by the two probes in the common frequency range. The results of this evaluation are reported in Appendix A. A possible explanation for this phenomenon could be a lower accuracy of the two probes for frequency points close to their operating boundaries. Nevertheless, for frequencies above 300 MHz, the DAK3.5 – TL2 seems to guarantee higher reliability by comparing the measurement data for well-known materials and the values reported in the literature for the same materials.

To assess the effect of uncertainties in dielectric properties arising both from manufacturing and from measurements, we performed a numerical validation. This validation

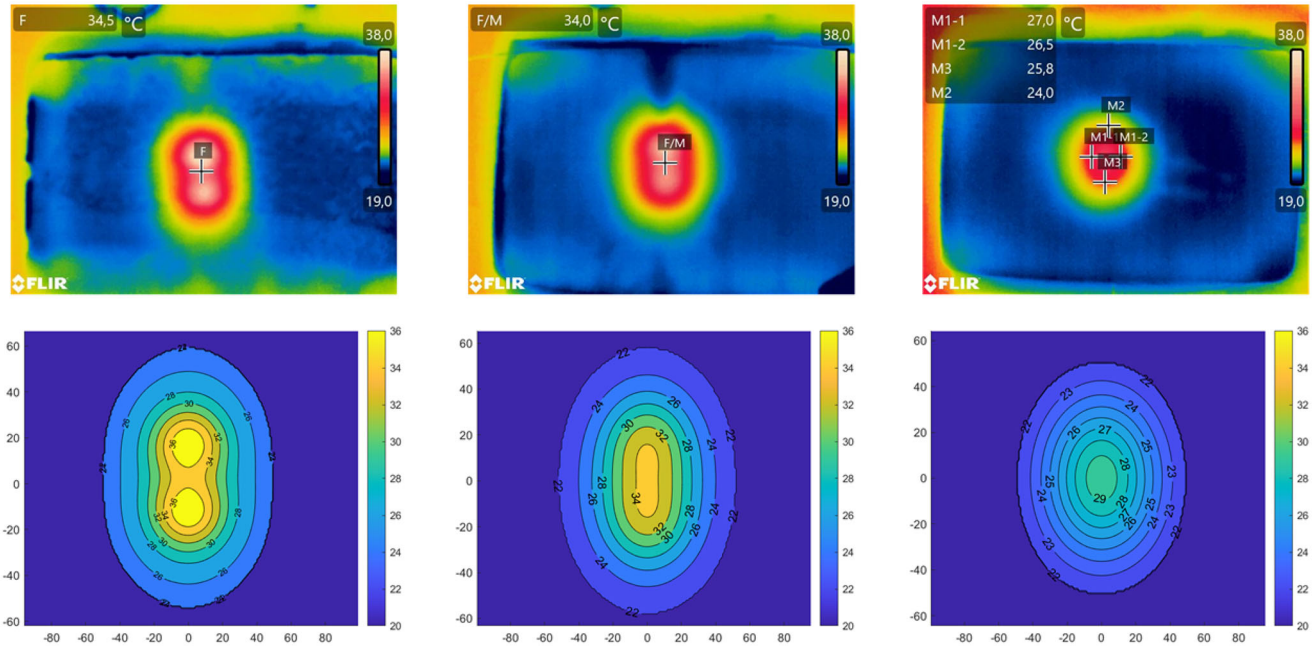


Figure 9. IR camera thermal images capturing the temperature distribution (top row) and simulated temperature levels after 6 min of exposure at 87 W (bottom row) at different interfaces. From the left to right: Fat/Fat, Fat/Muscle, Muscle/Muscle (1 cm deep). The markers on the thermal images correspond to the approximate position of the temperature sensors during the experiment.

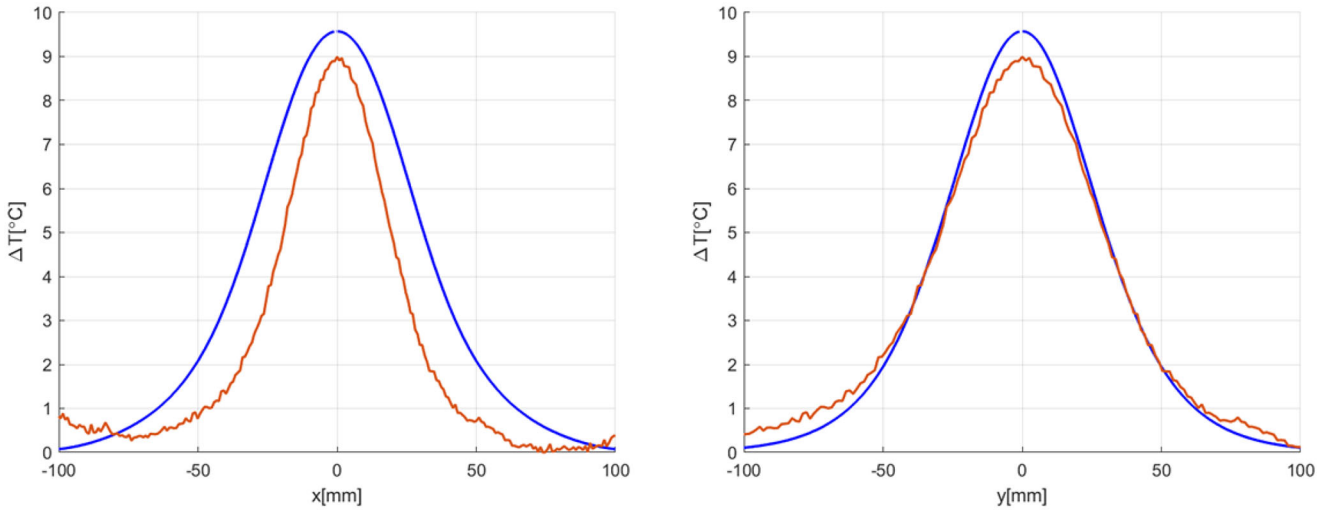


Figure 10. Comparison between the measured (orange line) and simulated (blue line) temperature increase along the y = 0 axis (left panel) and the x = 0 axis (right panel).

revealed that these uncertainties affect the power deposition only marginally. In the case of radiative systems operating at generally higher frequencies, deviations in all parameters were less than 5%, as shown in Table 4. For capacitive systems, the differences in EFS reach similar differences between 5-6%, but due to preferential heating of the fat at the fat-muscle boundary characteristic for the capacitive systems, the deviations in thermal quality indicators are larger. In the most extreme case of the LB dataset, the TEFS is overestimated by 13.7% while TEPD by 23.5%. In absolute measures, the variability of TEPD and TEFS translates to an acceptable 3 $cm^2$ and 3 mm, respectively.

The suitability of the proposed fat phantom for QA procedures was assessed experimentally with a radiative applicator and the results later compared with numerical data. The temperature rise after six minutes of heating satisfies the minimum requirements indicated in the QA guidelines [13]. The data recorded by the temperature probes and the IR camera show a temperature increase clearly below the setting of the material (91 °C). Overall, the phantom exhibits excellent mechanical stability up to temperatures close to 100 °C, without showing a clear melting point below 130 °C, as shown in Figure 6. The material also possesses great handling capabilities as shown in Figure 4. The 5-mm thick phantom was removed immediately after the execution of the QA experiment, sufficiently elastic to be moved without cracking. The lifetime has not yet been experimentally assessed, but its appearance and dielectric properties have not changed after several months. The absence of water in the recipe increases the microbiological stability and prevents changes in the phantom composition upon water evaporation.

## 5. Conclusions

We have demonstrated that glycerol-in-oil emulsions stabilized with EC can be adopted as fat-mimicking phantoms for hyperthermia QA procedures, even if with limitations in the low-frequency range (< 200 MHz). The manufacturing protocol is easily reproducible and contains affordable, accessible ingredients. The requirements on dielectric and thermal properties are also satisfied, although exhibiting low conductivity values for frequencies below 200 MHz. Despite the uncertainties on the dielectric properties, simulations showed an acceptable variability (within 5%) of different quality indicators (EFS, TEFS, TEPD) for radiative applicators. In the case of capacitive systems, the TEFS and TEPD are overestimated by 3 $cm^2$ and 3 mm, respectively, due to the low conductivity of the phantom. This represents a weakness to overcome, and a further experimental QA assessment involving capacitive systems is needed. The phantom shows excellent stability at high temperatures, proven both by the rheological assessments and the experimental QA testing, thus validating its usage in these procedures.

In conclusion, this work demonstrates the potential of the phantom to adequately represent both the dielectric and thermal properties of fat tissue, along with proper structural stability even at elevated temperatures. Therefore, we propose this fat tissue phantom for use in hyperthermia QA procedures, with limitations for usage in the lower clinical frequency bands.

## Disclosure statement

No potential conflict of interest was reported by the author(s).

## Funding

This research was funded by the European Union's Horizon 2020 research and innovation program under the Marie Skłodowska-Curie (MSCA-ITN) grant "Hyperboost" project, no. 955625, the Swedish Research Council grant number 2021-04935, an STSM grand under COST Action MyWAVE CA17115 and the Royal Irish Academy.

## ORCID

Mattia De Lazzari http://orcid.org/0000-0002-9736-5457
Anna Ström http://orcid.org/0000-0002-9743-1514
Laura Farina http://orcid.org/0000-0002-1571-8037
Sergio Curto http://orcid.org/0000-0002-3073-1117
Hana Dobšíček Trefná http://orcid.org/0000-0001-6025-0819

## Data availability statement

Raw data were generated at Chalmers University of Technology, Göteborg, and Eramsus MC, Rotterdam. Derived data supporting the findings of this study are available from the corresponding author H.D.T. on request.

## References

[1] Trefná HD, Crezee H, Schmidt M, et al. Quality assurance guidelines for superficial hyperthermia clinical trials:I. Clinical requirements. Int J Hyperthermia. 2017;33(4):471–482.
[2] Seegenschmiedt MH, Fessenden P, Vernon CC. Thermoradiotherapy and thermochemotherapy: biology. Physiology, physics. Vol. 1. 1995: Springer.
[3] Kato H, Hiraoka M, Ishida T. An agar phantom for hyperthermia. Med Phys. 1986;13(3):396–398.
[4] Kato H, Ishida T. Development of an agar phantom adaptable for simulation of various tissues in the range 5-40 mhz.(hyperthermia treatment of cancer). Phys Med Biol. 1987;32(2):221–226.
[5] Ito K, Furuya K, Okano Y, et al. Development and characteristics of a biological tissue-equivalent phantom for microwaves. Electron Comm Jpn Pt I. 2001;84(4):67–77.
[6] Nilsson P, Persson B, Kjellén E, et al. Technique for microwave-induced hyperthermia in superficial human tumours. Acta Radiol Oncol. 1982;21(4):235–239.
[7] Kuroda M, Kato H, Hanamoto K, et al. Development of a new hybrid gel phantom using carrageenan and gellan gum for visualizing three-dimensional temperature distribution during hyperthermia and radiofrequency ablation. Int J Oncol. 2005;27(1):175–184.
[8] Fontes-Candia C, Lopez-Sanchez P, Ström A, et al. Maximizing the oil content in polysaccharide-based emulsion gels for the development of tissue mimicking phantoms. Carbohydr Polym. 2021;256:117496.
[9] Bini MG, Ignesti A, Millanta L, et al. The polyacrylamide as a phantom material for electromagnetic hyperthermia studies. IEEE Trans Biomed Eng. 1984;31(3):317–322.
[10] Lazebnik M, Madsen EL, Frank GR, et al. Tissue-mimicking phantom materials for narrowband and ultrawideband microwave applications. Phys Med Biol. 2005;50(18):4245–4258.
[11] Yuan Y, Wyatt C, Maccarini P, et al. A heterogeneous human tissue mimicking phantom for RF heating and MRI thermal monitoring verification. Phys Med Biol. 2012;57(7):2021–2037.
[12] Madsen EL, Zagzebski JA, Frank GR. *Oil-in-gelatin dispersions for use as ultrasonically tissue-mimicking materials*. Ultrasound Med Biol. 1982;8(3):277–287.
[13] Dobšíček Trefná H, Crezee J, Schmidt M, et al. Quality assurance guidelines for superficial hyperthermia clinical trials: II. Technical requirements for heating devices. Strahlenther Onkol. 2017;193(5):351–366.
[14] Kato H, Hiraoka M, Nakajima T, et al. Deep-heating characteristics of an RF capacitive heating device. Int J Hyperthermia. 1985;1(1):15–28.
[15] Duan Q, Duyn JH, Gudino N, et al. Characterization of a dielectric phantom for high-field magnetic resonance imaging applications. Med Phys. 2014;41(10):102303.
[16] Lagendijk J, Nilsson P. Hyperthermia dough: a fat and bone equivalent phantom to test microwave/radiofrequency hyperthermia heating systems. Phys Med Biol. 1985;30(7):709–712.
[17] Tosh SM, Marangoni AG. Determination of the maximum gelation temperature in gelatin gels. Appl Phys Lett. 2004;84(21):4242–4244.
[18] Trefná HD, et al. Fat tissue equivalent phantoms for microwave applications by reinforcing gelatin with nanocellulose. Biomedical Physics & Engineering Express. 2021;7(6):065025.
[19] Kok H, Crezee J. A comparison of the heating characteristics of capacitive and radiative superficial hyperthermia. Int J Hyperthermia. 2017;33(4):378–386.
[20] Allen S, Kantor G, Bassen H, et al. CDRH RF phantom for hyperthermia systems evaluations. Int J Hyperthermia. 1988;4(1):17–23. assurance reports
[21] Nikawa Y, Chino M, Kikuchi K. Soft and dry phantom modeling material using silicone rubber with carbon fiber. IEEE Trans Microwave Theory Techn. 1996;44(10):1949–1953.
[22] Garrett J, Fear E. Stable and flexible materials to mimic the dielectric properties of human soft tissues. Antennas Wirel Propag Lett. 2014;13:599–602.
[23] Zetzl AK, Gravelle AJ, Kurylowicz M, et al. Microstructure of ethylcellulose oleogels and its relationship to mechanical properties. Food Structure. 2014;2(1-2):27–40.
[24] Fu H, Lo YM, Yan M, et al. Characterization of thermo-oxidative behavior of ethylcellulose oleogels. Food Chem. 2020;305:125470.
[25] Aguilar-Zárate M, Macias-Rodriguez BA, Toro-Vazquez JF, et al. Engineering rheological properties of edible oleogels with ethylcellulose and lecithin. Carbohydr Polym. 2019;205:98–105.
[26] Martı́nez M, et al. Influence of the concentration of a gelling agent and the type of surfactant on the rheological characteristics of oleogels. Il Farmaco. 2003;58(12):1289–1294.
[27] Stauffer PR, Rossetto F, Prakash M, et al. Phantom and animal tissues for modelling the electrical properties of human liver. Int J Hyperthermia. 2003;19(1):89–101.
[28] Faraone A, Balzano Q, Simunic D. Experimental dosimetry in a sphere of simulated brain tissue near a half-wave dipole antenna in 1998 IEEE EMC Symposium. International Symposium on Electromagnetic Compatibility. Symposium Record (Cat. No 98CH36253). 1998. IEEE.
[29] Gravelle AJ, Marangoni AG. Ethylcellulose oleogels: structure, functionality, and food applications. Adv Food Nutr Res. 2018;84:1–56.
[30] Wasilewska K, Winnicka K. Ethylcellulose–a pharmaceutical excipient with multidirectional application in drug dosage forms development. Materials. 2019;12(20):3386.
[31] Vrba J, Vrba D. Temperature and frequency dependent empirical models of dielectric properties of sunflower and olive oil. Radioengineering. 2013;22(4):1281–1287.
[32] Pecovska-Gjorgjevich M, Andonovski A, Velevska J. Measuring frequency-and temperature-dependent permittivities of vegetable oils. Physica Macedonica. 2010;59:77–89.
[33] Lizhi H, Toyoda K, Ihara I. Dielectric properties of edible oils and fatty acids as a function of frequency, temperature, moisture and composition. J Food Eng. 2008;88(2):151–158.
[34] Praveen Kumar AV, Goel A, Kumar R, et al. Dielectric characterization of common edible oils in the higher microwave frequencies using cavity perturbation. J Microw Power Electromagn Energy. 2019;53(1):48–56.
[35] Meaney PM, Fox CJ, Geimer SD, et al. Electrical characterization of glycerin: water mixtures: implications for use as a coupling medium in microwave tomography. IEEE Trans Microw Theory Tech. 2017;65(5):1471–1478.
[36] De Lazzari M, et al. Design and manufacture procedures of phantoms for hyperthermia QA guidelines, in *EuCAP 2023*. 2023. Florence.
[37] Farina L, Sumser K, van Rhoon G, et al. Thermal characterization of phantoms used for quality assurance of deep hyperthermia systems. Sensors. 2020;20(16):4549.

[38] Silva NP, Bottiglieri A, Conceição RC, et al. Characterisation of ex vivo liver thermal properties for electromagnetic-based hyperthermic therapies. Sensors. 2020;20(10):3004.
[39] TEMPOS user manual. Pullman (WA): METER Group Inc.; 2018.
[40] Hasgall PA, Baumgartner DGF, Neufeld C, et al. *IT'IS Database for thermal and electromagnetic parameters of biological tissues*. Version 4.1; 2022. Available from: itis.swiss/database.
[41] Takook P, Persson M, Gellermann J, et al. *Compact self-grounded Bow-Tie antenna design for an UWB phased-array hyperthermia applicator*. Int J Hyperthermia. 2017;33(4):387–400.
[42] *CST studio suite* 2020. ® - *3D EM simulation and analysis software, Dassault Systemes, France*. Available from: https://www.3ds.com/products-services/simulia/products/cst-studio-suite/.
[43] *COMSOL Multiphysics® v. 6.0.* Stockholm (Sweden): COMSOL AB; 2022. Available from: www.comsol.com.
[44] Trefná HD, Ström A. Hydrogels as a water bolus during hyperthermia treatment. Phys Med Biol. 2019;64(11):115025.
[45] Gabriel C. Compilation of the dielectric properties of body tissues at RF and microwave frequencies. 1996. King's Coll London (United Kingdom Dept of Physics).

## Appendix A: verification of the DAK 12/3.5 TL-2 dielectric probes uncertainty

Permittivity and conductivity of pure liquid glycerol, purchased from VWR Chemicals, Radnor, Pennsylvania, USA, have been measured over the 8–600 MHz and 200 MHz – 1 GHz frequency ranges using, respectively, the DAK 12-TL2 and DAK 3.5-TL2 probes, provided by Speag. Prior to the measurements of the samples, the system has been calibrated according to the manufacturer's indications, following an open-short-load routine. Deionized water and a 0.1 molar saline (NaCl) solution have been employed as loads for the DAK 3.5-TL2 and DAK 12-TL2 probes, respectively.

The glycerol was poured into the provided Petri dishes and left covered in the room for 1h to guarantee the thermic equilibrium with the surrounding environment.

The measurement results are reported in Figure 1. As can be observed, a systematic difference which varies between 5% and15% between the values measured with the probes is present, both for conductivity and permittivity in the common frequency band.

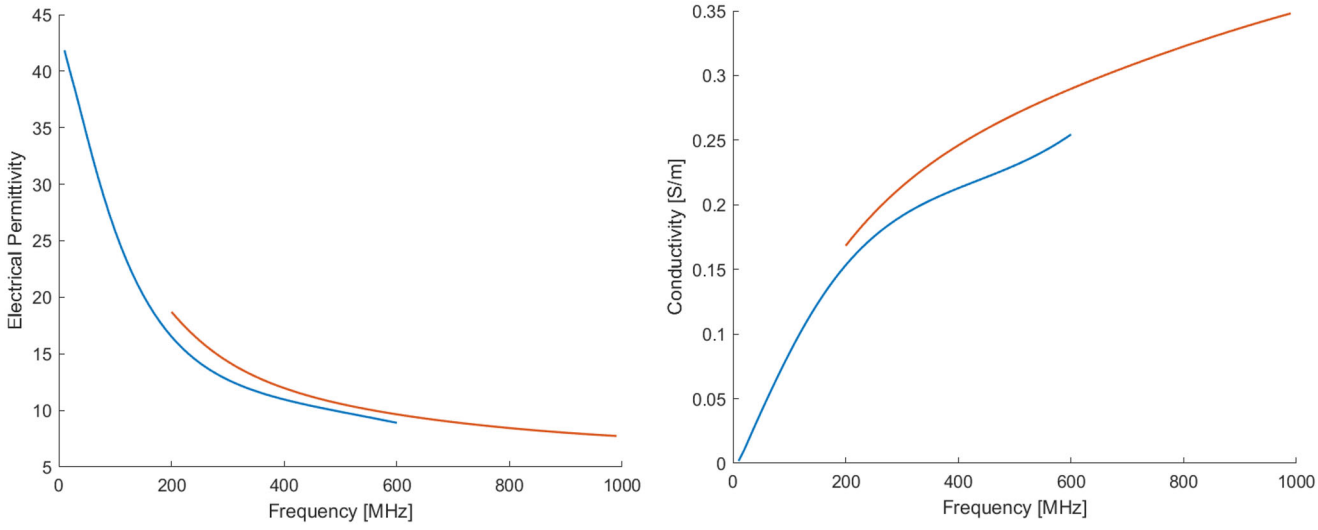


Figure A1. Permittivity and conductivity measured on a sample of pure glycerol using the DAK12 – TL2 (blue line) and the DAK3.5 – TL2 (orange line) probes.